1. On the γ-phase

The γ-phase forms an ordered layer structure in $P2_1/n$, $Z = 4$, with one molecule per asymmetric unit. The monoclinic lattice parameters at room temperature are $a = 10.8222(3)$ Å, $b = 24.1690(15)$ Å, $c = 8.3623(5)$ Å, $\alpha = \gamma = 90°$, $\beta = 100.576(3)°$, $V = 2150.1(2)$ Å^3. The layers are parallel to (3 0 $\bar{1}$). If the unit cell is transformed with **a'** = **a** + 3 **c**, **b'** = **b**, **c'** = **c**, the (0 0 1) plane becomes parallel to the layers and the space group changes to $P2_1/a$, $Z = 4$, with $a = 25.4328$ Å, $b = 24.1690$ Å, $c = 8.3623$ Å, $\alpha = \gamma = 90°$, $\beta = 24.727°$, $V = 2150.1$ Å^3. The layers are not planar, but wavy, as shown in Fig. S1c and Fig. S1d.

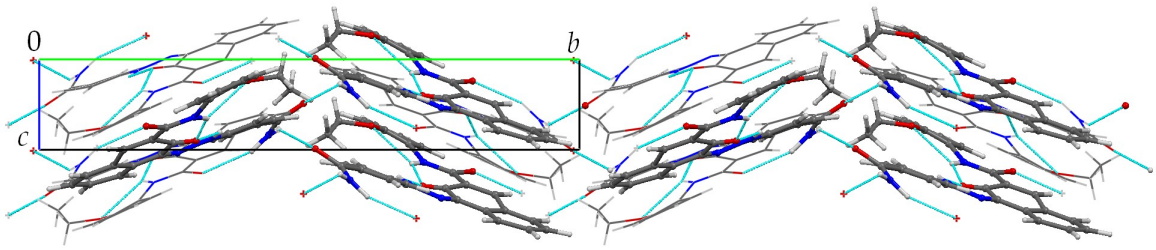

a)

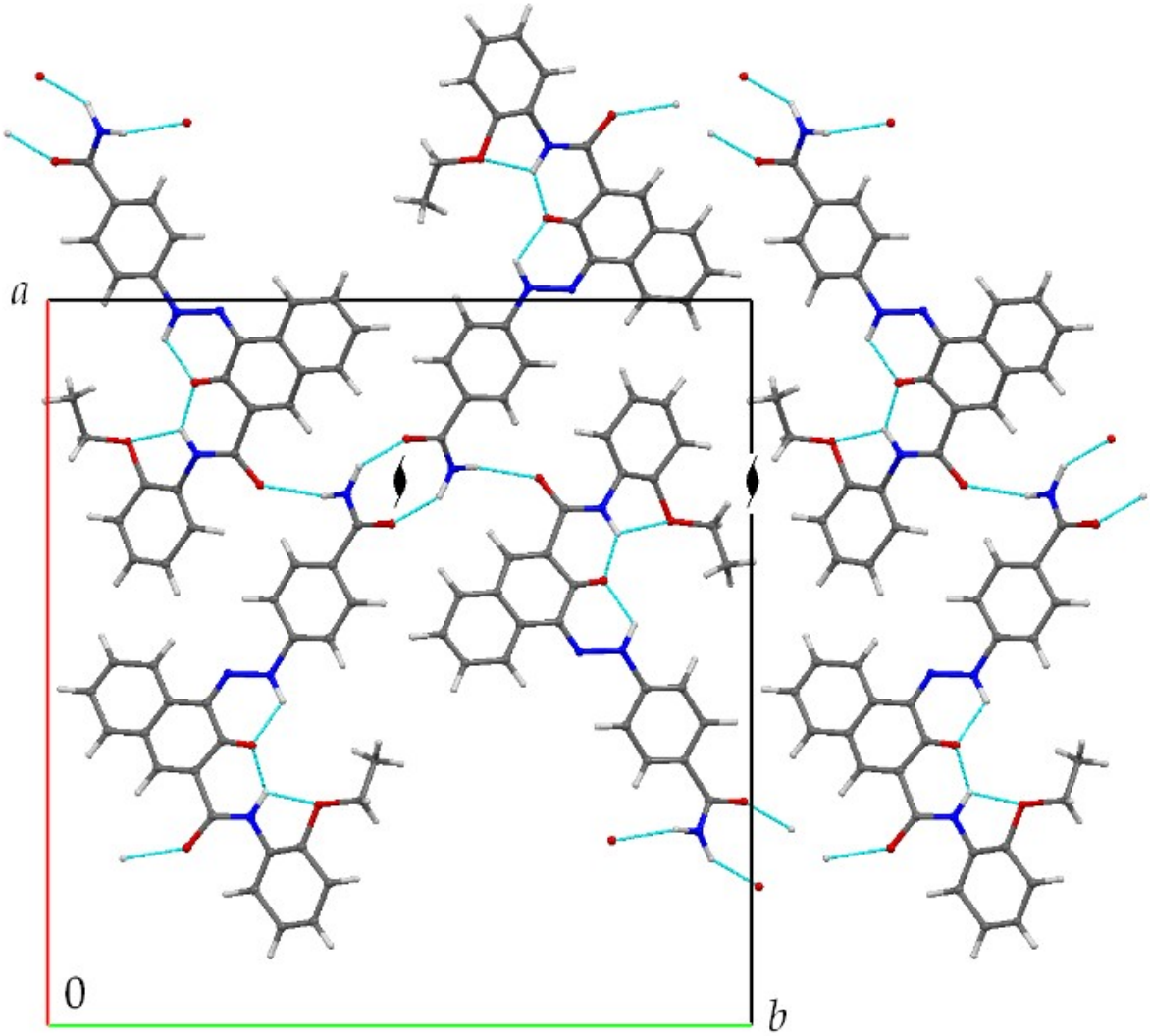

b)

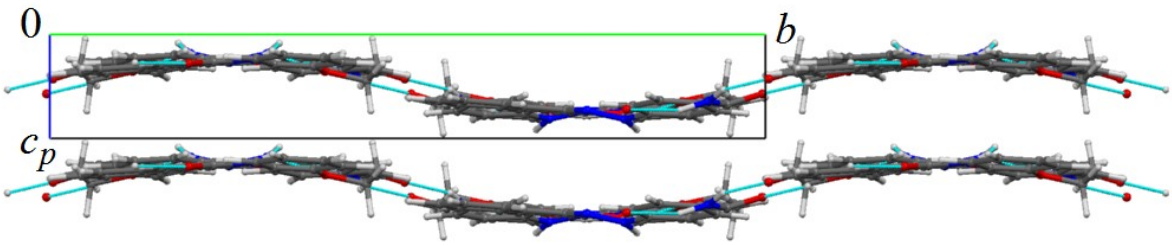

c)

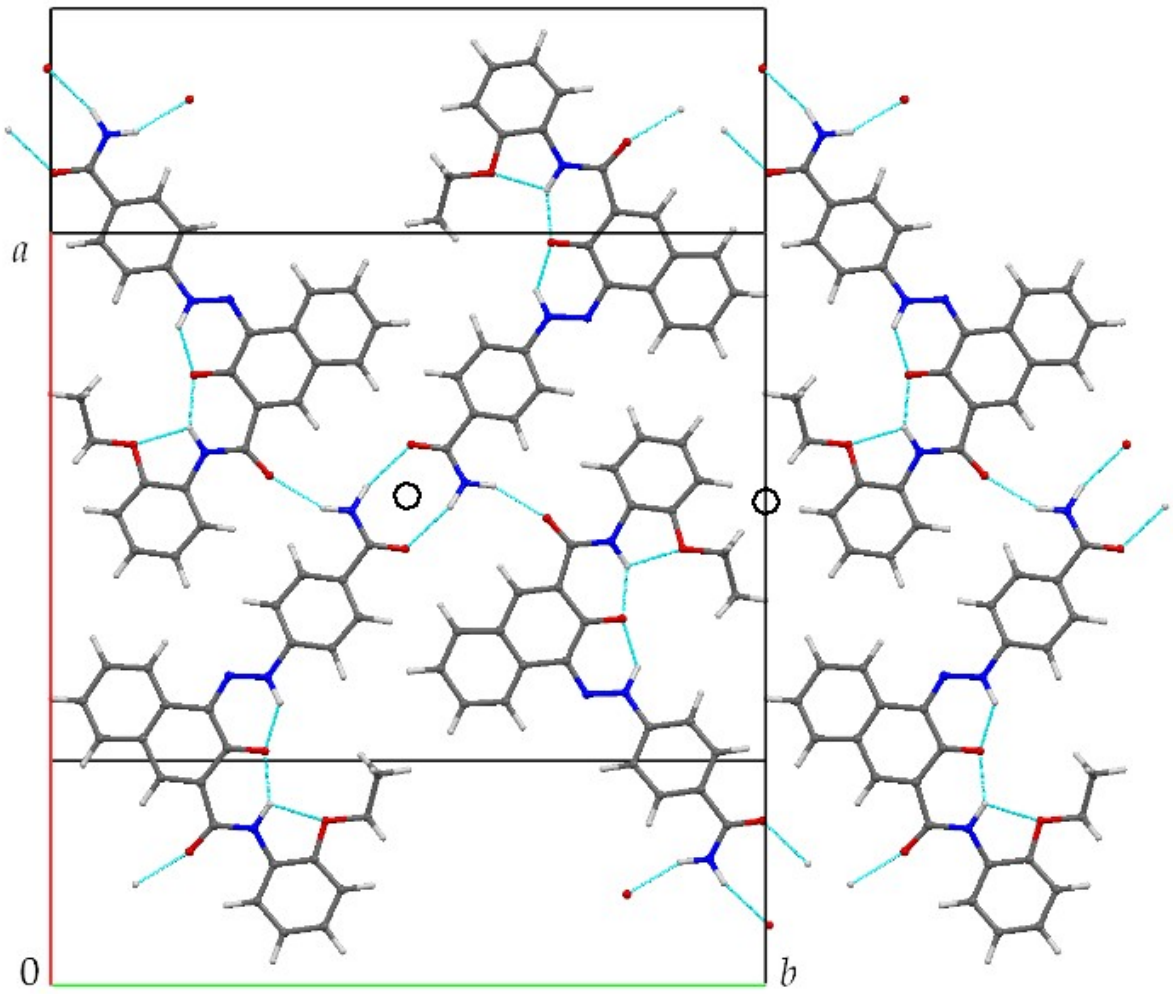

d)

Figure S1: Crystal structures of P.R. 170:

a) α-phase, view direction [$\bar{1}$ 0 0]; b) α-phase, view direction [0 0 1];

c) γ-phase after cell transformation, view direction [$\bar{1}$ 0 0];

d) γ-phase after cell transformation, view direction down **c***.

In the α-phase the $CONH_2$ groups form helices around twofold screw axes, in the γ-phase the $CONH_2$ groups form dimers via inversion centres (denoted by circles).

1.1. On order and disorder in the α- and the γ-phases of P.R.170

The α-phase (Schmidt *et al.*, 2006) is not disordered because of the herringbone arrangement (see Fig. S1a, b); the hydrogen bonds between the layers fix the lateral positions of neighbouring layers and do not allow any ambiguity.

The γ-phase (Schmidt *et al.*, 2006) possesses a layer structure similar to the β-phase. However, the

assembly of wavy layers would allow only a translational shift in the **a** direction, i.e. orthogonal to both the layer stacking direction and that of the waves, in the transformed γ-phase unit cell (see Fig. S1c, d). However, lattice-energy minimisations show that models with different shifts in the [1 0 0] direction either converge back to the structure of the γ-phase or result in strongly distorted layer geometries with very unfavourable energies.

2. Average structure models

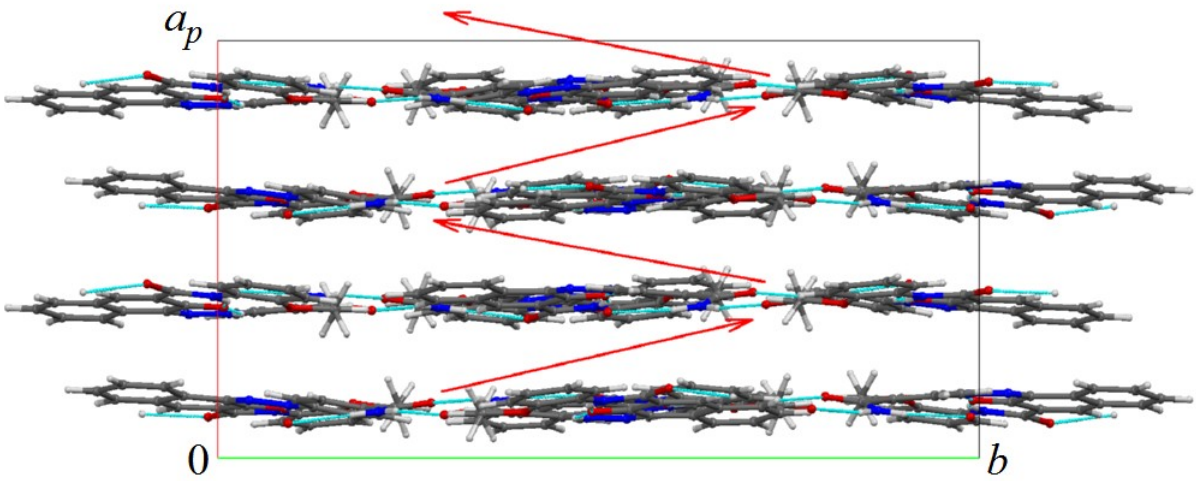

a)

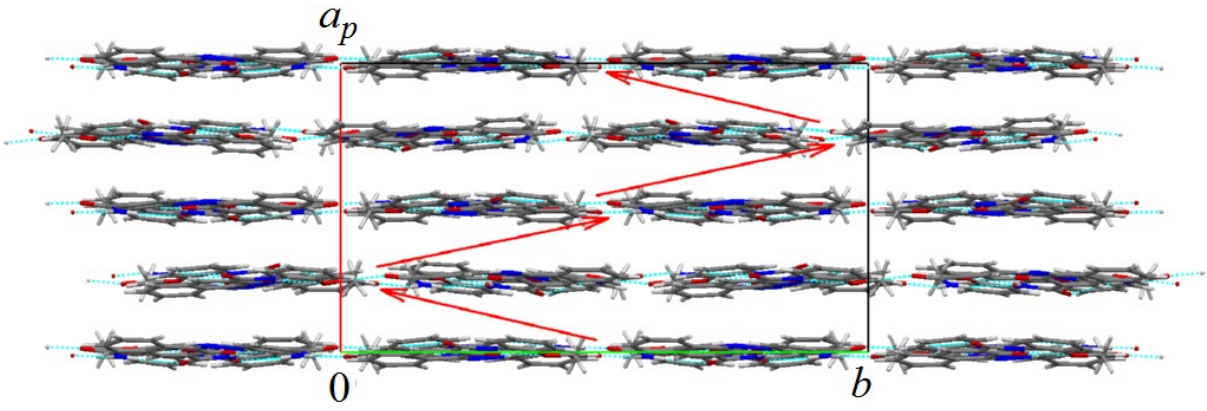

b)

Figure S2: Models of the average structure of the β-phase of P.R. 170. Direction of view: down [0 0 1]. a) major occupied positions in model **1**; b) full and major occupied positions in model **2**. The red arrows denote the translation vectors between the layers (compare Fig. 7).

3. Details on the lattice-energy minimisations

3.1. Atomic charges fitted from electrostatic potential

Atomic charges for Pigment Red 170 were tested on the known ordered phases with structures determined by Schmidt *et al.*, 2007. Charges were calculated with the 6-311G** basis set (McLean & Chandler, 1980). Two methods were used to fit atomic charges to the electrostatic potential: the Merz-Kollman method after Besler *et al.* (1990), and the CHelpG method after Breneman & Wiberg (1990), both implemented in Gaussian 03 (Frisch *et al.*, 2004). With both methods the atomic charges were constrained to reproduce the dipole moment of the molecule.

Surprisingly, using the CHelpG atomic charges resulted in heavily distorted molecule and layer geometries for the α-phase model with a disastrous r.m.s.d. value of 5.93 Å for atomic positions. For the energetically favourable structure of the γ-phase using the CHelpG atomic charges yields an acceptable r.m.s.d. value of 0.254 Å. In an equally surprising manner, lattice-energy minimisations with these atomic charges and the Dreiding force field also yielded a more favourable lattice energy for the α-phase than for the γ-phase, which directly contradicts the experimentally observed phase stabilities. In an additional calculation CHelpG atomic charges were assigned to a basic ordered model of the β-phase, which underwent a lattice-energy minimisation. This calculation yielded a triclinic unit cell with a heavily distorted "saw-tooth" layer geometry. Neither the cell metrics nor the layer geometry correspond to any known solid-state phase of P.R. 170. These results prompted the dismissal of CHelpG atomic charges as infeasible for the task at hand.

Atomic charges calculated with the Merz-Kollman method after Besler *et al.*, 1990, were used for all further calculations. These charges yield a vastly improved r.m.s.d. value of 1.07 Å for the α-phase and a comparable r.m.s.d. value of 0.30 Å for the γ-phase and allow a good reproduction of the experimentally determined layer geometry and occupied positions in the β-phase.

3.2. Tailor-made force field parameters

The parameter (X – N_R – C_R – X), which describes the torsion around any nitrogen-carbon bond in a conjugated system, was changed from 25 to 30 kcal/mol. New parameters were added to describe the planar hydrazone group between the aromatic rings. A torsion parameter (N_R – N_R – C_R – C_R), which describes the specific torsion around the hydrazone nitrogen-carbon bond, was set up at 35 kcal/mol. An angle bend parameter (C_R – C_R – N_R) which describes the bond angles at the carbon atoms carrying the hydrazone group, was set up at 150 kcal mol^{-1} rad^{-2} with a

default angle of 120°.

The resulting parametrisation was tested on similar hydrazone compounds with known ordered crystal structures. Atomic charges were calculated for each molecule with the 6-311G** basis set using the Merz-Kollman method and constrained to the dipole moment of the molecule.

The lattice-energy minimisations with Merz-Kollman atomic charges reproduced the molecular structures and crystal structures of these pigments with good accuracy, including intramolecular and intermolecular hydrogen-bonds and molecular orientations relative to the layer planes. R.m.s.d. values of non-hydrogen atoms were calculated after van de Streek & Neumann, 2010. A detailed listing of the hydrazone compounds used is given in table S1.

Table S1: Hydrazone compounds and r.m.s.d. values.

Compound (CSD entry)	Structure published by	r.m.s.d. value / Å
ANACMO	Kobelt *et al.*, 1972	0.270
CABWAE	Yatsenko *et al.*, 2001	0.162
CICCUN	Schmidt *et al.*, 2007	0.249
CIPGMR10	Paulus, 1982	0.140
MNIPZN	Whitaker, 1978	0.093
OLOCAT	Chang *et al.*, 2003	0.114
UJIGAW	Das & Biswas, 2010	0.124
VEHXIP	Gridunova *et al.*, 1989	0.115
VEHXOV	Gridunova *et al.*, 1989	0.119

3.3. On the lattice-energy minimisations

Lattice-energies were also calculated for the known structures of the α- and the γ-phases. Phase transition experiments show that the α-phase is the least stable and the γ-phase is the most stable phase of P.R. 170, since the α-phase converts into the other two phases and the β-phase converts into the γ-phase under thermodynamic conditions. The obtained lattice-energies are in agreement with the experimental stabilities, with the α-phase having the highest and γ-phase the lowest lattice-energy. The various models for the β-phase are in between the other phases.

In several large models of P.R.170 a partial transition from the β-phase to the more favourable stackings similar to other models or similar to the γ-phase was observed regardless of fixed lattice parameters: During the optimisation, the layers shifted along the [0 1 0] axis, while the layer

geometry changed from planar (as in the β-phase) to wavy (as in the γ-phase). These models were disregarded from further analyses.

4. X-ray powder diffraction and electron microscopy

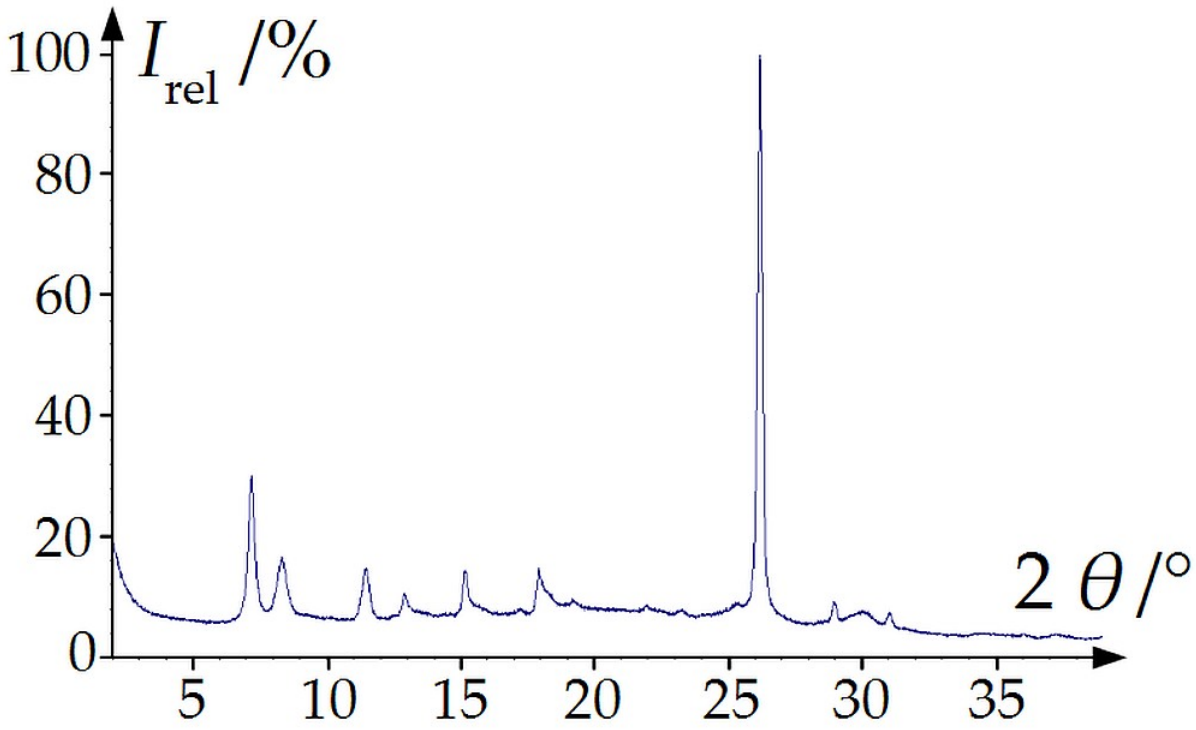

Figure S3. X-ray powder diffraction diagram of β-P.R.170 at 100K (λ = 1.5406 Å; Sample II from isobutanol treatment).

Exposure to X-ray radiation for 24 hours confirmed that no phase transition or sample damage occurs during the diffraction experiments. The powder pattern cannot be indexed directly, so an immediate structure solution is not possible. Nevertheless, we tried to solve the structure by crystal-structure prediction performing lattice-energy minimisations in various space groups with free lattice parameters, using the programs FleXCryst and CRYSCA. For all low-energy structures X-ray powder diagrams were simulated and compared with the experimental powder diagram. In the case of the α-phase this method was successful, although the powder data were only partially indexed (**a***, **b***, γ* from indexing; **c***, α*, β* unknown). However, none of the calculated structures gave a powder diagram which reproduced the experimental diagram of the β-phase. Nevertheless, Rietveld refinements of several calculated structures were tried, but none of them gave a reasonable fit to the experimental powder data.

Several derivatives were synthesised with the hope of finding an isostructural compound with improved crystallinity. This attempt had been successful for the α-phase (by using a methyl derivative), but none of the synthesised derivatives was isostructural with the β-phase. Similarly, solid solutions were tried in order to improve the crystallinity; but also this approach was unsuccessful.

4.1. Comparison between X-ray single-crystal and powder diffraction data

A powder diagram was simulated from the single-crystal diffraction data recorded by Warshamanage *et al.* (2013) by spherically integrating the full diffraction pattern, including the diffuse scattering, without any prior extraction of individual reflection intensities. The resulting powder diffraction pattern is in fairly good agreement with the experimental powder pattern (Fig. S4a, d).

On the other hand, powder patterns were simulated from the average structure models **1** and **2**. Good agreement of these simulated powder diffraction patterns with the experimental powder diffraction pattern (Fig. S4b, c, d) shows that the structure of the single crystal corresponds well with the crystal structure of the powder sample.

The simulated powder diagrams of models **1** and **2** differ mainly in the intensity of the reflection at $2\theta = 13°$, which is the 2 0 0 reflection.

Additionally, we constructed a model with 100 layers assuming a purely random sequence of layers. The simulated powder diagram is shown in Fig. S4e; however, additional reflections appear in the diffraction pattern (indicated by arrows). This again proves that the layer stacking deviates significantly from just being random.

The experimental powder diagram (Fig. S4d) shows only a few reliable reflections. This low number explains why all attempts to index the X-ray powder diagram from scratch failed. In an unbiased indexing a monoclinic unit cell with a volume of more than 3500 $Å^3$ and $Z' = 2$, as found by Warshamanage *et al.* (2013), would be considered as highly speculative for a powder pattern containing only about 15 reflections. Furthermore, from this powder diagram a crystal structure with at least two independent molecules would have never been solved by any method. Also crystal-structure prediction by lattice-energy minimisations with subsequent simulation of the powder patterns could not solve the structure, because we did not include structures with $Z' = 2$; and with $Z' = 1$ the correct structures could not have been found.

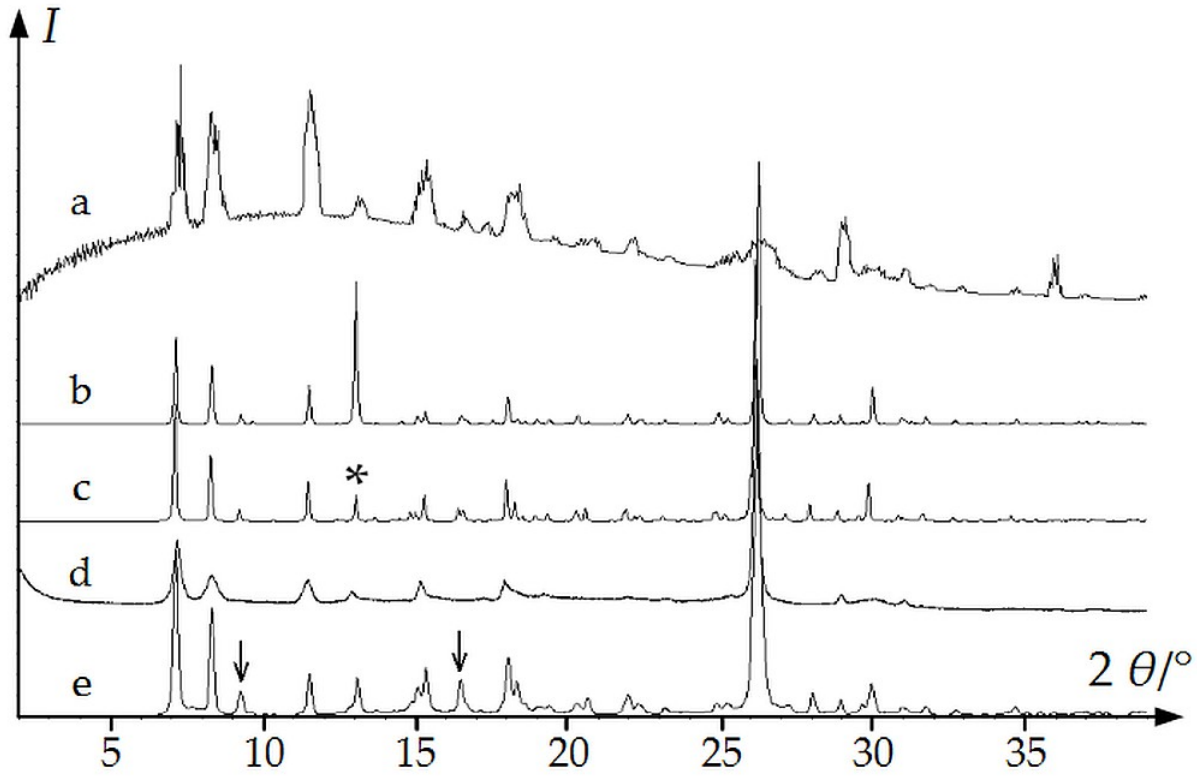

Figure S4. X-ray powder diffraction patterns. All patterns recorded at 100 K.

From top to bottom:

a) Pattern calculated by spherical integration of single-crystal diffraction data from sample III;

b) simulated pattern from model **2**;

c) simulated pattern from model **1**; the 2 0 0 reflection is indicated by *;

d) experimental powder pattern of sample II;

e) simulated pattern of a model containing 100 layers with a fully random sequence; two reflections, absent in the experimental powder diffraction pattern, are indicated by arrows.

4.2. Electron microscopy

Typically, directions associated with large lattice vectors or disorder are least developed directions in crystal morphology. Thus these directions tend to arrange along the electron beam when the crystals are placed onto the carbon film. On the other hand, the direction corresponding with the stacking of molecular layers is typically one of the longest crystal dimensions – for instance, the needle axis. Therefore, for β-P.R.170 the diffuse streaks do not run parallel to the electron beam, but are arranged more or less along the needle-axis of the crystals, and thus could be directly recorded in electron diffraction.

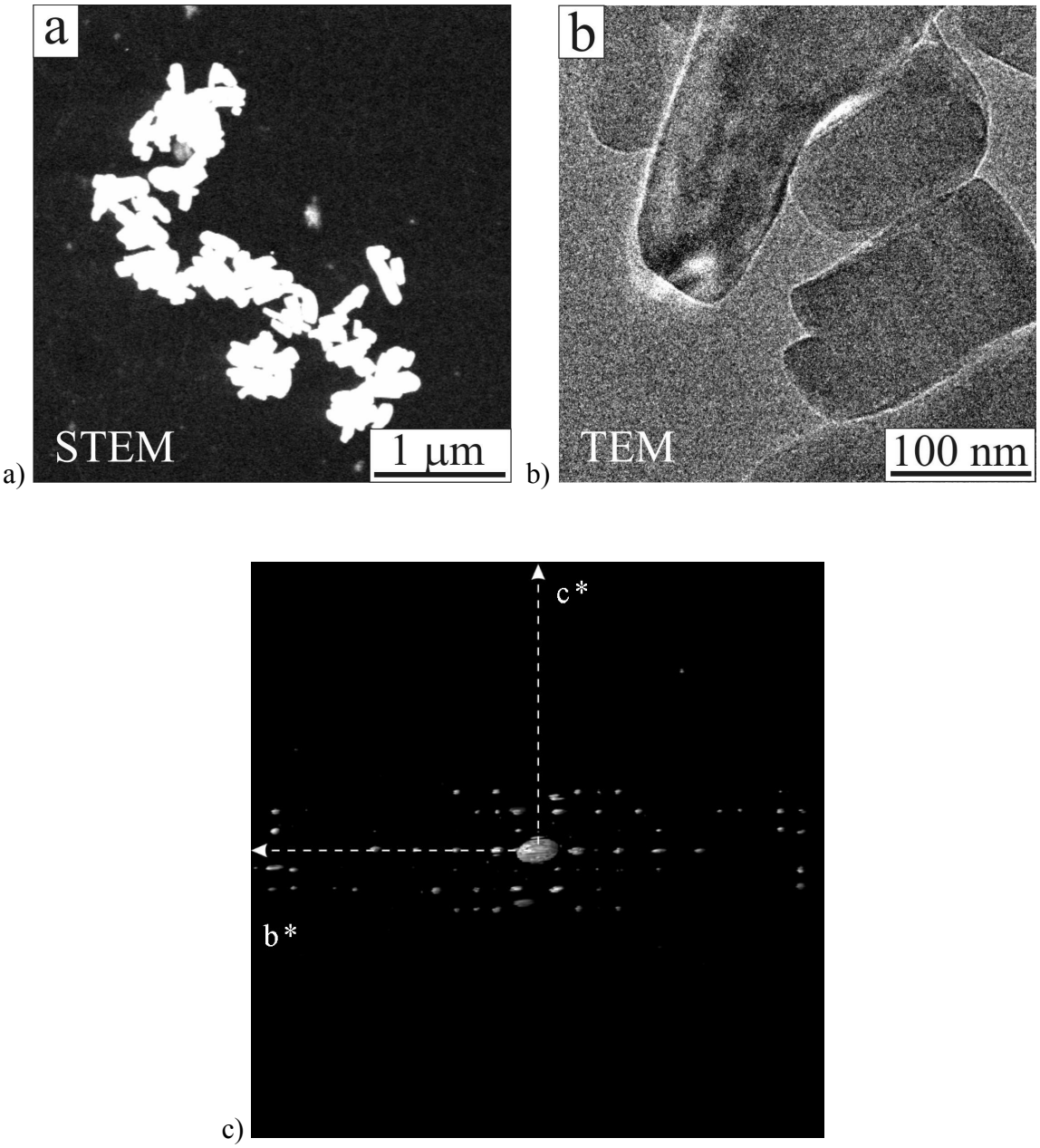

a) b) c)

Figure S5. a) STEM images of crystals of β-P.R.170 from sample I.
b) TEM images of crystals of β-P.R.170 from sample I.
c) Projection of three-dimensional diffraction data reconstructed from ADT data.
View orthogonal to the (0 0 1) plane.

5. Layers, layer stacking and stacking disorder

5.1. On the occupancies

The experimentally observed occupancies of molecular sites in model **1** are about 93% vs. 7%. In contrast the occupancies in model **2** are 100% vs. 65% vs. 35%. Do these values contradict each other? Let's make the following *Gedankenexperiment:*
Let's consider a structure which only contains the small zigzag (+ −) and the large zigzag (+ + − −) motifs. A 40-layer structure with a sequence '+ − + − + − + − + − + − + − + − + − + − + − + − + − + − + − + + − − + + − − + + − −' corresponds in model **1** to '99 99 99 99 99 99 99 99 99 99 99 99 99 99 99 9199 9199 9199'. This sequence contains 93% layers of the „9“ type and 7% layers of the „1“ type, which is in exact agreement with the experimental occupancies. The same sequence is described in model **2** as '6f 3f 6f 3f 6f 3f 6f 3f 6f 3f 6f 3f 6f 3f 6f6f 6f6f 6f6f ' and contains 50% of fully occupied layers „f“; from the remaining layers there are 65% of type „6“ and 35% of type „3“, which is again in perfect agreement with experimentally observed occupancies of about 65% and about 35%. A real crystal obviously contains other sequences as well; however this *Gedankenexperiment* illustrates that the different occupancies in models **1** and **2** are not contradictory to each other. If the occupancies in model **1** are given as A vs. (1-A) and in disordered layers of model **2** as B vs. (1-B) then the occupancies are related by B = 2.5 – 2A.

5.2. Single molecule; single layer

The molecular geometry from the single-crystal structure analysis is well reproduced by the force-field calculations. The force-field geometry of the molecule is in similarly good agreement with the ab initio calculations. This proves that the modifications made on the intramolecular parameters of the force-field were successful.

5.3. Additional stacking possibilities

Occupying only the minor (0.07) positions in model **1** would result in the periodic sequence '11', which is less favourable than the sequence '99' by 10.27 kJ/mol. An incorporation of a '...11...' fragment into larger sequences does not change the situation: The sequence '991199' is worse than '991919' by 2.13 kJ/mol; this value is averaged over six shifts and corresponds for a single shift to an energy loss of 12.78 kJ/mol caused by the '11' transition. Similarly high energy losses of 10.78 kJ/mol are found for the '11' fragment in '99119999' against '91999199', and of 14.11 kJ/mol

for '9911' against '9191'. Consequently, all following discussions were restricted to structures with $t_y = \pm 0.421$, i.e. to sequences with **'+'** and **'−'** shifts only.

If the layers were planar, there would be two additional MDO structures. Repeated application of the screw axis parallel to **a*** results in '+ q + q' (or '− p − p'); repeated application of the diagonal glide plane perpendicular to **c** would result in the sequence '+ p + p' (or '− q − q'). These MDO structures are energetically unfavourable, see section 3.3.2 of the main paper.

5.4. Influence of neighbouring layers

Within the layers the molecules are held together by van der Waals interactions, Coulomb interactions and hydrogen bonds. Hence significant in-plane motions or rotations of individual molecules relative to neighbouring molecules are hardly possible. In contrast, the molecules may bend or tilt out of the plane without significant energy loss, as observed in the calculation of a single-layer in the gas phase, as well as in the crystal structures of the α- and γ-phases consisting of non-planar layers. However, in all calculations of the β-phase, as well as in the X-ray experiments, the layers are almost planar. This is a packing effect, caused by the surrounding layers.

The lattice-energy minimisations show that the actual geometry of the layers changes very slightly with the arrangement of neighbouring and next-neighbouring layers. The geometry of a layer surrounded by two equal layers (e.g. 9**9**9 pattern in the sequence '9991') deviates slightly from the geometry of a layer surrounded by two different layers (e.g. 1**9**9 pattern in the sequence '9199'). A superposition of the geometries of these layers is shown in Fig. S6.

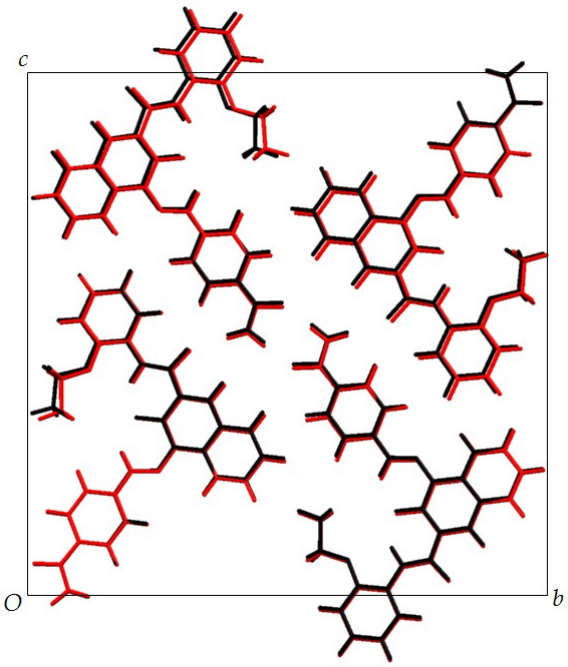

Figure S6. Influence of the neighbouring layers on the local structure.

Red: geometry of a layer surrounded by two equal layers (9**2**9 pattern).

Black: geometry of a layer surrounded by two different layers (1**2**9 pattern). View along ***a****.

Hence the influence of the arrangement of the layers on the local structure of the layers themselves is relatively small. In the single-crystal X-ray structure analysis, larger deviations of the atomic positions in different layers would lead to split atomic positions or strongly anisotropic displacement parameters (ADP) in the average structure. The fact, that the local structure is similar in all layers, explains the absence of such "strange" ADPs in the experimental X-ray structures.

5.5. Influence and interactions of next-neighbouring layers

There are two possible arrangements for next-neighbouring layers: 1) the third layer is above the first one ($\Delta y = 0$); 2) the third layer is shifted ($\Delta y = \pm 0.842$). In all cases Δz is equal to 0.5. The interactions between the first and the third layer consist of two parts: a) conveyed by the second layer; b) direct through-space Coulomb and van der Waals interactions.

The direct through-space interactions were calculated after removal of the intervening second layer. If the third layer is above the first one, the energy is more favourable, the Coulomb energy by 0.6-0.9 kJ/mol and the van der Waals energy by up to 0.15 kJ/mol; both values depend slightly on the layer geometries, which are affected by the individual stacking sequence.

Apart from this energetic effect, the next-neighbouring layers have a visible influence on the geometry of the layer. For example, the geometry of a layer sandwiched by two equal layers (9**9**9 pattern) depends on the next-neighbouring layers (99**9**99 vs. 19**9**91) as shown in Fig. S7. The maximum observed deviation of the carbon atom positions is approx. 0.3 Å.

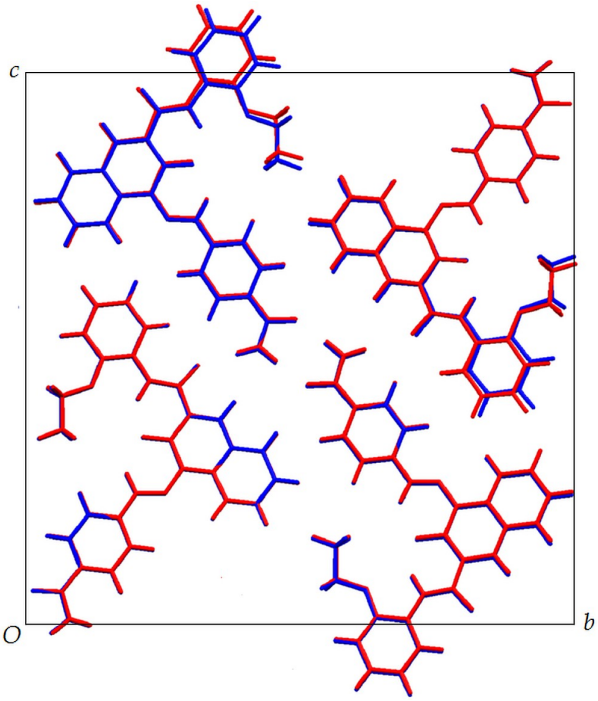

Figure S7. Influence of next-neighbouring layers on the local structure.

Red: geometry of the third layer in the 99**9**99 pattern.

Blue: geometry of the third layer in the 19**9**91 pattern. View along **a***.

5.6. Why is the crystal structure monoclinic?

If all possible stacking sequences are constructed, using a combinatorial approach, there are 4 possibilities for a two-layer sequence ('+ −', '− +', '+ +', '− −'), of which two pairs are symmetry-equivalent ('+ −' and '− +'; '+ +' and '− −'). For a 4-layer sequence there are already $2^4 = 16$ possibilities, of which four are symmetry-independent; for 6-layer models eight of 64 are different (see Table 1). Those sequences which contain an equal number of '+' and '−' vectors, can be derived from both model **1** and model **2** while featuring new layer positions. Other sequences, with unequal numbers of '+' and '−' shifts, result in deviations from monoclinic metrics, and therefore cannot be described as an ordered variant of either model **1** or model **2**. As apparent from the 4-layer and 6-layer models in Table 2, the structures with equal numbers of '+' and '−' shifts (or, at least, an almost

equal number) have better energies.

Statistical analysis of the stacking sequences obviously shows that twinned sequences, e.g. '+ + +' and '− − −' have equal probabilities of occurring and equal probabilities of being followed by an appropriately twinned layer, i.e. the sequence '+ + + −' is as probable as '− − − +'; the sequence '+ + + +' is as probable as '− − − −'. Therefore, for a sufficiently large crystal domain, the overall numbers of '+' and '−' layer shifts are equal, yielding an overall monoclinic structure.

5.7. Local stacking probabilities

For the stacking sequences, an additive combination of energies is assumed, i.e. the energy of a given layer is defined by selected surrounding layers. Such distinctive finite-shift sequences are defined as patterns. For a given pattern length, the overall number of possible patterns is determined combinatorially. The number of symmetry-independent patterns is limited by the symmetry conditions.

The energy of a model of any given sequence can then be described as the sum of such patterns' energies. This allows for a mathematical approach to determine separate pattern energies from their linear combinations, which have been calculated beforehand as model energies. Within a combinatorially complete set of models the pattern energies, the model energies and the linear combinations of patterns assigned to models form an over-defined system of linear equations. As such systems do not permit exact solutions, a least-squares method is used to obtain the best approximations for pattern energies.

The Boltzmann distribution is applied to obtain probabilities for these patterns, yielding first the relative occupancy values N_i and then probabilities p_i for each pattern. Probabilities calculated by this method describe the chances to find certain combinations of neighbouring and next-neighbouring layers within a theoretical infinite disordered crystal. Thus the local structure is determined.

The resulting probabilities are given in Table S2.

Table S2: Probabilities for local stacking motifs (pattern) containing 4 layers.

a) Derived from periodic 4-layer models			
Pattern	Pattern energy kJ/mol	Degeneracy of pattern	Probability of pattern
+ + +	-0.04	2	0.1380
+ + − = − + +	-2.12	4	0.6405
− + −	-1.21	2	0.2215

b) Derived from periodic 6-layer models			
Pattern	Pattern energy kJ/mol	Degeneracy of pattern	Probability of pattern
+ + +	-0.18	2	0.1527
+ + − = − + +	-1.92	4	0.6161
− + −	-1.21	2	0.2312

The pattern probabilities from different combinatorially complete sets of models are in good agreement. The accuracy of the determined probabilities increases with the number of models in the set, as larger systems of equations allow for better least-squares solutions.

A supercell model containing 100 layers was constructed to approximately represent the average structure model **1** by randomly placing 90% of the layers on the major occupied position and placing the remaining 10% of the layers on the minor occupied position. This approach hence yields a 100 layer model with a random layer sequence.

On the other hand, the above stacking pattern probabilities were used to construct a 100-layer structural model with regards to the local structure. Both 100-layer models yield 99 superstructure reflections between neighbouring Bragg reflections parallel to the **a*** direction in the simulated diffraction pattern. These superstructure reflections overlap and give a good representation of the diffuse streaks.

References

Besler, B. H., Merz, Jr. K. M. & Kollman, P. A. (1990). *J. Comp. Chem.* **11**, 431-39.

Breneman, C. M. and Wiberg, K. B. (1990). *J. Comp. Chem.*, **11**, 361-73.

Chang, C.-H., Christie, R. M., Rosair, G. M.(2003). *Acta Cryst. C* **59**, o556-o558.

Christie, R. M. (2002). Presentation on the Colorchem'02, 9th international conference on dyes and pigments, 12-16 May 2002, Špindlerův Mlýn, Czech Republic.

Das, P. & Biswas, A. N., (2010). *J. Chem. Cryst.* **40**, 1167-1169.

Frisch, M. J., Trucks, G. W., Schlegel, H. B., Scuseria, G. E., Robb, M. A., Cheeseman, J. R., Montgomery, Jr. J. A., Vreven, T., Kudin, K. N., Burant, J. C., Millam, J. M., Iyengar, S. S., Tomasi, J., Barone, V., Mennucci, B., Cossi, M., Scalmani, G., Rega, N., Petersson, G. A., Nakatsuji, H., Hada, M., Ehara, M., Toyota, K., Fukuda, R., Hasegawa, J., Ishida, M., Nakajima, T., Honda, Y., Kitao, O., Nakai, H., Klene, M., Li, X., Knox, J. E., Hratchian, H. P., Cross, J. B., Bakken, V., Adamo, C., Jaramillo, J., Gomperts, R., Stratmann, R. E., Yazyev, O., Austin, A. J., Cammi, R., Pomelli, C., Ochterski, J. W., Ayala, P. Y., Morokuma, K., Voth, G. A., Salvador, P., Dannenberg, J. J., Zakrzewski, V. G., Dapprich, S., Daniels, A. D., Strain, M. C., Farkas, O., Malick, D. K., Rabuck, A. D., Raghavachari, K., Foresman, J. B., Ortiz, J. V., Cui, Q., Baboul, A. G., Clifford, S., Cioslowski, J., Stefanov, B. B., Liu, G., Liashenko, A., Piskorz, P., Komaromi, I., Martin, R. L., Fox, D. J., Keith, T., Al-Laham, M. A., Peng, C. Y., Nanayakkara, A., Challacombe, M., Gill, P. M. W., Johnson, B., Chen, W., Wong, M. W., Gonzalez, C., & Pople, J. A. (2004). Gaussian 03, Revision B.01, *Gaussian Inc.*, Wallingford CT, 2004.

Gridunova, G. V., Ezhkova, Z. I., Shklover, V. E., Struchkov, Yu. T., Sycheva, E. D., Lisitsyna, E. S., Grigor'eva, L. P. (1989). *Russ. J. Org. Chem.* **25**, 583-591.

Hofmann, D. W. M. & Apostolakis, J. (2003). *J. Mol. Struc. (Theochem)*, 647, 17-39.

Kobelt, D., Paulus, E. F., Kunstmann, W. (1972). *Acta Cryst. B* **28**, 1319-1324.

McLean, A. D., & Chandler, G. S. (1980). *J. Chem. Phys.*, **72**, 5639-48.

Paulus, E. F. (1982). *Z. Kristallogr.* **160**, 235-243.

Schmidt, M. U., Buchsbaum, C., Schnorr, J. M., Hofmann, D. W. M. & Ermrich, M. (2007). *Z. Kristallogr.* **222**, 30-33.

Schmidt, M. U., Hofmann, D. W. M., Buchsbaum, C. & Metz, H. J. (2006). *Angew. Chem.* **118**, 1335-1340, *Angew. Chem. Int. Ed.,* **45**, 1313-1317.

Schmidt, M. U., Kalkhof, H. (1997-2003). CRYSCA, Program for Crystal Structure Calculation of flexible molecules, Frankfurt am Main.

Van de Streek, J., Neumannn, M. A. (2010). *Acta Cryst.*, **B66**, 544–558.

Warren, B. E. (1969). X-Ray Diffraction, pp. 227-245, *New York: Dover Publications, Inc.*, New York, USA.

Warshamanage, R., Bürgi, H.-B., Schmidt, M. U. & Linden, A. (2013). *Acta Cryst. B.* Submitted.

Whitaker, A. (1978). *Z. Kristallogr.* **147**, 99-112.

Yatsenko, A. V., Paseshnichenko, K. A., Chernyshev, V. V., Schenk, H. (2001). *Acta Cryst. E* **57**, o1152-o1153.